

# Quest of $^{37}\text{Mg}$ halo structure using Glauber model and microscopic relativistic mean field densities

Mahesh K. Sharma\* and Manoj K. Sharma

*School of Physics and Materials Science, Thapar University, Patiala - 147 004, Punjab, India*

R. N. Panda

*Department of Physics, ITER, Siksha O Anusandhan University, Bhubaneswar-751 030, India*

S. K. Patra

*Institute of Physics, Sahcivalaya marg Bhubaneswar-751 005, India*

(Dated: September 17, 2018)

We have studied the ground state properties (binding energy and charge radius) using relativistic mean field formalism (RMF) for Mg-isotopes in the valley of stability to drip line region. The RMF densities have been analyzed in context of reaction dynamics. The calculated results of  $^{24-40}\text{Mg}+^{12}\text{C}$  reactions at projectile energy 240 A MeV using Glauber model with the conjunction of densities from relativistic mean field formalism are compared with experimental data. We found remarkable agreement of estimated values of reaction cross sections with experimental data except for  $^{37}\text{Mg}$  isotope. In view of this, the halo status of  $^{37}\text{Mg}$  is examined through higher magnitude of rms radius and small value of longitudinal momentum distribution. Finally, an effort is made to explore the structure of  $^{37}\text{Mg}$  halo candidate using Glauber few body formalism.

PACS numbers: 25.60.Pj, 25.70.Gh, 25.70.Jj, 27.90.+q

## I. INTRODUCTION

Since last few decades, the advent in radioactive ion beam facilities, the drip line physics and structure of drip line nuclei got large attention by the nuclear science community. The advancement in these facilities enrich our knowledge toward the new exotic phenomena such as one and two neutron/proton halo, bubble effect in densities, vanishing of shell closer effect at the drip line region and identification of some new magic numbers for the deformed configuration etc. The understanding of above mention concepts strengthen our understanding in the island of inversion. One of the most exotic phenomenon that have been exploited extensively toward drip line is halo status of nuclei. The halo structure originates due to extremely weak bound nucleons which decouple from the nuclear core. The interaction cross sections of such nuclei like  $^6,8\text{He}$ ,  $^{11}\text{Li}$  and  $^{11,14}\text{Be}$  [1] are anomalously high due to large magnitude of consolidated root mean square (rms) radii. The one neutron/proton breakup of halo projectiles with stable target at near/far barrier energies is one of the tool to investigate the structure of such systems [2]. The measurement of longitudinal momentum distribution for  $^{16-18}\text{C}$  isotopes after one-neutron breakup from  $^{17-19}\text{C}$  isotopes using the fragment separator observed narrow value of full width half maximum (FWHM) for  $^{18}\text{C}$  ( $\sim 44.3 \pm 5.9$  MeV/c), which indicates that  $^{19}\text{C}$  is a one-neutron halo [3]. In addition to this, the measurement of nuclear reaction cross-sections for  $^{19,20,22}\text{C}$  [4, 5] show that the drip-line nucleus  $^{22}\text{C}$  has a

halo structure. The one and two neutron removal cross sections and momentum distribution give indication for the halo status of a nuclear system. It is relevant to mention that  $^{22}\text{C}$  has  $N = 16$  which is a new magic number in neutron-rich region [6, 7] and forms a Borromean halo structure ( $^{21}\text{C}$  is unstable). It is of large interest to study the existence of bound states of two nucleons (neutrons or protons) with core in the Borromean structure, which have not appeared in vacuum. Soon after  $^{31}\text{Ne}$  was included in the family of neutron halo. The measurement of interaction cross sections for Ne isotopes from the stability line to neutron drip line at 240 MeV/nucleon energy [8], show the dependence of mass number for  $^{27-32}\text{Ne}$  isotopes, which have been explained by nuclear deformations. The enhancements of interaction cross sections particularly for  $^{29}\text{Ne}$  and  $^{31}\text{Ne}$  have been quoted by an s-dominant halo structure of  $^{29}\text{Ne}$  and s- or p-orbital halo in  $^{31}\text{Ne}$  [9]. The isotope  $^{31}\text{Ne}$  having neutron number  $N=21$ , seem to break the shell closer structure. As a consequence, a large value of deformation associated with the strong intruder configuration put in at "island of inversion".

Recently, M. Takechi et al. [10], have measured the data of reaction cross section for Mg isotopes at energy 240 A MeV at RIBF and RIKEN. In this study, they have observed large reaction cross section value for  $^{37}\text{Mg}$  as compared to other isotopic chain and consequently predicted  $^{37}\text{Mg}$  to have a halo structure. In another study S. Watanabe [11] concluded from their fully microscopic double folding frame work with the AMD densities, that  $^{37}\text{Mg}$  exhibits deformed halo structure. In our earlier work we explored the structure of some isotopes of Ne, Mg and Si [12]. The identification of this new candidate as halo encourage us to review our study for Mg isotopes.

---

\*maheshphy82@gmail.com

Therefore we have made a motivated effort to study the reaction dynamics of Mg isotopes at energy 240 AMeV. A sincere effort is made to analyze the structural features of  $^{37}\text{Mg}$ . The reaction/interaction cross section, angular elastic differential cross section, one nucleon removal cross section and angular momentum distributions parameters are exercised for the analysis of such nuclear systems.

The section II contains a brief description of Glauber formalism. Section III describe the calculations and results, and finally a summary and conclusions is described in the section IV.

## II. THE FORMALISM

We use the well known Glauber approach to investigate reaction dynamics [13–15]. The study of reaction dynamics in the framework of this approach strongly depends on the densities of the projectile and target nuclei, and we have used the microscopic relativistic mean field (RMF) densities with NL3 parameter [16].

### A. Glauber Model

#### 1. Reaction cross section

The theoretical formalism to study the reaction cross sections using the Glauber approach has been given by R. J. Glauber [13]. The standard Glauber form for total reaction cross sections is expressed as [13, 14]

$$\sigma_R = 2\pi \int_0^\infty b[1 - T(b)]db, \quad (1)$$

where 'T(b)' is the Transparency function with impact parameter 'b'. The function T(b) is calculated by

$$T(b) = \exp\left[-\sum_{i,j} \sigma_{ij} \int \bar{\rho}_{tj}(s) \bar{\rho}_{pi}(|\vec{b} - \vec{s}'|) d\vec{s}'\right]. \quad (2)$$

Here, the summation indices i, j run over proton and neutron and subscript 'p' and 't' refers to projectile and target respectively.  $\sigma_{ij}$  is the experimental nucleon-nucleon reaction cross-section which depends on the energy. The z- integrated densities are defined as

$$\bar{\rho}(\omega) = \int_{-\infty}^{\infty} \rho(\sqrt{w^2 + z^2}) dz, \quad (3)$$

with  $\omega^2 = x^2 + y^2$ . Initially Glauber model was designed for the high energy approximation. However, it was found to work reasonably well for both the nucleus-nucleus reaction and the differential elastic cross-sections over a broad energy range [15, 17]. The modified transparency function T(b) is given by

$$T(b) = \exp\left[-\int_p \int_t \sum_{i,j} [\Gamma_{ij}(\vec{b} - \vec{s}' + \vec{t}')] \bar{\rho}_{pi}(\vec{t}') \bar{\rho}_{tj}(\vec{s}') d\vec{s}' d\vec{t}'\right]. \quad (4)$$

The profile function  $\Gamma_{NN}$  for optical limit approximation is defined as

$$\Gamma_{NN} = \Gamma_{ij}(b_{eff}) = \frac{1 - i\alpha_{NN}}{2\pi\beta_{NN}^2} \sigma_{NN} \exp\left(-\frac{b_{eff}^2}{2\beta_{NN}^2}\right), \quad (5)$$

for finite range and

$$\Gamma_{NN} = \Gamma_{ij}(b_{eff}) = \frac{1 - i\alpha_{NN}}{2} \sigma_{NN} \delta(b), \quad (6)$$

for zero range with  $b_{eff} = |\vec{b} - \vec{s}' + \vec{t}'|$ ,  $\vec{b}$  is the impact parameter. Where  $\vec{s}'$  and  $\vec{t}'$  are the dummy variables for integration over the z-integrated target and projectile densities. The parameters  $\sigma_{NN}$ ,  $\alpha_{NN}$  and  $\beta_{NN}$  usually depend upon the proton-proton, neutron-neutron and proton-neutron interactions. Here  $\sigma_{NN}$  is the total nuclear reaction cross section of NN collision,  $\alpha_{NN}$  is the ratio of the real to the imaginary part of the forward nucleon-nucleon scattering amplitude and  $\beta_{NN}$  is the slope parameter. The slope parameter determines the fall of the angular distribution of the N-N elastic scattering.

#### 2. Angular elastic differential cross section

The nucleus-nucleus elastic scattering amplitude is written as

$$F(q) = \frac{iK}{2\pi} \int db e^{iq \cdot b} (1 - e^{i\chi(b)}). \quad (7)$$

At low energy, this model is modified in order to take care of finite range effects in the profile function and Coulomb modified trajectories. The elastic scattering amplitude including the Coulomb interaction is expressed as

$$F(q) = e^{i\chi_s} \left\{ F_{coul}(q) + \frac{iK}{2\pi} \int db e^{iq \cdot b + 2i\eta \ln(Kb)} (1 - e^{i\chi(b)}) \right\}, \quad (8)$$

with the Coulomb elastic scattering amplitude

$$F_{coul}(q) = \frac{-2\eta K}{q^2} \exp\left\{-2i\eta \ln\left(\frac{q}{2K}\right) + 2i \arg \Gamma(1 + i\eta)\right\}, \quad (9)$$

where  $K$  is the momentum of projectile and  $q$  is the momentum transferred from the projectile to the target. Here  $\eta = Z_P Z_T e^2 / \hbar v$  is the Sommerfeld parameter,  $v$  is the incident velocity of the projectile, and  $\chi_s = -2\eta \ln(2Ka)$  with  $a$  being a screening radius. The elastic differential cross section is given by

$$\frac{d\sigma}{d\Omega} = |F(q)|^2. \quad (10)$$

$$\frac{d\sigma}{d\sigma_R} = \frac{|F(q)|^2}{|F_{coul}(q)|^2}. \quad (11)$$

### 3. one nucleon removal cross section

The one nucleon removal cross section,  $\sigma_{-N}$ , may be defined as

$$\sigma_{-N} = \Sigma_c \int dk \sigma_{a=(k,g=0),c} \quad (12)$$

we assume that the core remains in its ground state,  $g=0$ . The one nucleon removal cross section consists of both elastic and inelastic part and can be calculated by

$$\sigma_{-N} = \sigma_{-N}^{el} + \sigma_{-N}^{inel}. \quad (13)$$

The cross section due to the elastic breakup process is given by

$$\sigma_{-N}^{el} = \int db \{ \langle \phi_0 | e^{-2Im\chi_{CT}(b_c) - 2Im\chi_{NT}(b_c+s)} | \phi_0 \rangle - | \langle \phi_0 | e^{i\chi_{CT}(b_c) + i\chi_{NT}(b_c+s)} | \phi_0 \rangle |^2 \}. \quad (14)$$

While the cross section from inelastic breakup is given by

$$\sigma_{-N}^{inel} = \int db \{ \langle \phi_0 | e^{-2Im\chi_{CT}(b_c) - e^{-2Im\chi_{CT}(b_c) - 2Im\chi_{NT}(b_c+s)} | \phi_0 \rangle \}. \quad (15)$$

### 4. Longitudinal momentum distribution

The momentum distribution of core after the inelastic breakup of Projectile reads as:

$$\frac{d\sigma_{-N}^{inel}}{dP} = \int \frac{dq}{K^2} \sum_{c \neq 0} \int dk \delta(P - \frac{A_C}{A_P} \hbar q + \hbar K) |F_{(K,0)_c}(q)|^2 \quad (16)$$

The Scattering wave function of nucleon is approximated by a plane wave reduced to

$$\frac{d\sigma_{-N}^{inel}}{dP_{||}} = \int db_N (1 - e^{-Im\chi_{NT}(b_N)}) \times \frac{1}{(2\pi\hbar)^3} \frac{1}{2j+1} \sum_{mm_s} \left| \int dr e^{\frac{i}{\hbar} P \cdot r} \chi_{\frac{1}{2}m_s} e^{i\chi_{CT}(b_N-S)\varphi_{nljm}(r)} \right|^2, \quad (17)$$

where  $b_N$  stands for the impact parameter of valence nucleon with respect to the target. The longitudinal momentum distribution obtained by the integration of above equation over transverse component of momentum  $P_{\perp}$ , gives.

$$\begin{aligned} \frac{d\sigma_{-N}^{inel}}{dP_{||}} &= \int dP_{\perp} \frac{d\sigma_{-N}^{inel}}{dP} \\ &= \frac{1}{2\pi\hbar} \int db_N (1 - e^{-2Im\chi_{NT}(b_N)}) \int ds e^{-2Im\chi_{CT}(b_N-s)} \\ &\quad \times \frac{1}{(2l+1)} \left| \int dz e^{\frac{i}{\hbar} P_{||} z} u_{nlj}(r) Y_{lm_l}(\hat{r}) \right|^2. \quad (18) \end{aligned}$$

### B. Relativistic mean field formalism

The relativistic mean field approach is well documented in Refs. [18–22]. The basic ingredient of RMF model is the relativistic Lagrangian density for a nucleon-meson many body system which is defined as [20]

$$\begin{aligned} \mathcal{L} &= \bar{\psi}_i (i\gamma^\mu \partial_\mu - M) \psi_i + \frac{1}{2} \partial^\mu \sigma \partial_\mu \sigma \\ &\quad - \frac{1}{2} m_\sigma^2 \sigma^2 - \frac{1}{3} g_2 \sigma^3 - \frac{1}{4} g_3 \sigma^4 - g_s \bar{\psi}_i \psi_i \sigma \\ &\quad - \frac{1}{4} \Omega^{\mu\nu} \Omega_{\mu\nu} + \frac{1}{2} m_\omega^2 V^\mu V_\mu \\ &\quad - g_\omega \bar{\psi}_i \gamma^\mu \psi_i V_\mu - \frac{1}{4} \vec{B}^{\mu\nu} \cdot \vec{B}_{\mu\nu} \\ &\quad + \frac{1}{2} m_\rho^2 \vec{R}^\mu \cdot \vec{R}_\mu - g_\rho \bar{\psi}_i \gamma^\mu \vec{\tau} \psi_i \cdot \vec{R}^\mu \\ &\quad - \frac{1}{4} F^{\mu\nu} F_{\mu\nu} - e \bar{\psi}_i \gamma^\mu \frac{(1 - \tau_{3i})}{2} \psi_i A_\mu. \quad (19) \end{aligned}$$

Here  $\sigma$ ,  $V_\mu$  and  $\vec{R}_\mu$  are the fields for  $\sigma$ -,  $\omega$ - and  $\rho$ -meson respectively.  $A^\mu$  is the electromagnetic field. The  $\psi_i$  are the Dirac spinors for the nucleons whose third component of isospin is denoted by  $\tau_{3i}$ .  $g_s$ ,  $g_\omega$ ,  $g_\rho$  and  $\frac{e^2}{4\pi} = \frac{1}{137}$  are the coupling constants for the linear term of  $\sigma$ -,  $\omega$ - and  $\rho$ -mesons and photons respectively.  $g_2$  and  $g_3$  are the parameters for the non-linear terms of the  $\sigma$ -meson.  $M$ ,  $m_\sigma$ ,  $m_\omega$  and  $m_\rho$  are the masses of the nucleons,  $\sigma$ -,  $\omega$ - and  $\rho$ -mesons, respectively.  $\omega^{\mu\nu}$ ,  $\vec{B}^{\mu\nu}$  and  $F^{\mu\nu}$  are the field tensors for the  $V^\mu$ ,  $\vec{R}^\mu$  and the photon fields, respectively. The quadrupole moment deformation parameter  $\beta_2$ , root mean square radii and binding energy are evaluated using the standard relations [18]. The nuclear density  $\rho = \sum_{i=1}^A \psi_i^\dagger \psi_i$  is obtained by solving the equation of motion obtained from the above Lagrangian. The values of the parameters for NL3 are given as [16]  $g_s=10.217$ ,  $g_\omega=12.868$ ,  $g_\rho=4.574$ ,  $g_2 = -10.431$  ( $f m^{-1}$ ),  $g_3 = -28.885$ , and  $M=939$ ,  $m_\sigma=508.194$ ,  $m_\omega=782.501$ ,  $m_\rho=763.0$  in MeV.

### III. CALCULATIONS AND DISCUSSION

The ground state properties of Mg-isotopes are calculated using microscopic relativistic mean field formalism. Fig 1 shows the calculated values of binding energy (B. E.) and charge radius ( $r_c$ ) of considered set of isotopes of Mg. The lower panel of the figure shows the calculated values of B.E, which find nice comparison with experimental data which looks nice agreement with each others. A deep inspection of the figure shows that the B. E.'s slightly under estimate up to the  $^{29}\text{Mg}$  and overestimate beyond  $^{32}\text{Mg}$  isotopes. While the upper panel of figure compare the calculated value of rms charge radius ( $r_c$ ) of considered set of isotopes with the experimental data. The calculated values of  $r_c$  are underestimated in comparison to experimental data. The success of relativistic

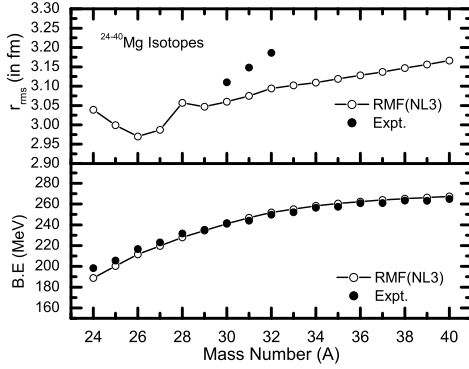


FIG. 1: The values of B.E in MeV and Charge radius of Mg isotopes after obtained from RMF(NL3) as a function of mass number (A). The experimental data are also given for comparison whichever be available.

mean field formalism depends on the appropriate choice of densities and we have used RMF(NL3) densities as an input of Glauber model.

In the measurement of reaction parameter through Glauber formalism, one of the input for evaluation of profile function in Glauber model is its energy as well as isospin dependent parameters. The values of these parameter at  $E_{Proj}=240$  AMeV are  $\sigma_{NN}=3.266868$  ( $fm^2$ ),  $\alpha_{NN}=0.6800303$  and  $\beta_{NN}=0.097843707$  ( $fm^2$ ). These values have been estimated by spline interpolation from Ref. [23]. Other important inputs of Glauber model are the densities of the projectile and the target nuclei. Fig. 2 shows the relativistic mean field (RMF) densities of projectiles with NL3 parameter set, which shows the density profile as a function of radial distance for  $^{24-40}$ Mg nuclei. Here the nucleonic densities distribution are of larger values at the center and goes on decreasing as the radius increases. where the small depletion in densities also appear at the center for these nuclei. One may also observed from the figure that the skin effect increases with increase of isotopic mass number.

These densities can be feed as an input of Glauber model after converting into spherical equivalent of it in terms of Gaussian coefficients. We have converted these densities into Gaussian form and calculated their values in terms of Gaussian coefficients  $c_i$ 's and  $a_i$ 's using relation:

$$\rho(r) = \sum_{i=1}^n c_i \exp[-a_i r^2], \quad (20)$$

The Gaussian coefficients which are used as input in the Glauber model code [24] are listed in Table 1 for NL3 interaction.

For the address of reaction dynamics, the single particle wave function is used in Glauber model. The radial part of single particle wave function have been obtained after solving Schrodinger equation using Wood-Saxon type potential as in the form:

$$U(r) = -v_0 f(r) + V_{ls}(l.s) r_0^2 \frac{1}{r} \frac{df(r)}{dr} + V_{Coul}, \quad (21)$$

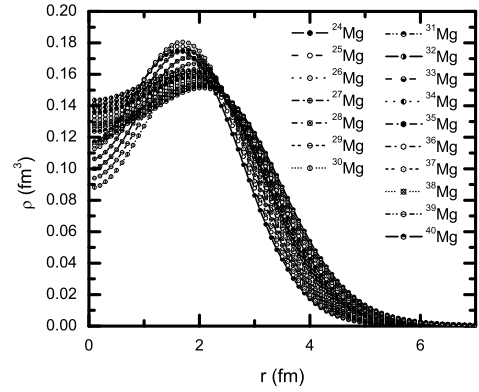


FIG. 2: The density profile of Mg isotopes from RMF(NL3) formalism as a function of radial distance.

TABLE I: The Gaussian coefficients for the Projectile and Target after fitting RMF(NL3) densities are listed in Table below.

Nuclei	RMF(NL3)			
	$c_1$	$a_1$	$c_2$	$a_2$
$^{12}C$	-0.232654	0.638687	0.517232	0.339911
$^{24}Mg$	-3.6936	0.286163	3.80452	0.261585
$^{25}Mg$	-3.89231	0.281947	4.00019	0.258213
$^{26}Mg$	-4.07533	0.277958	4.18027	0.25493
$^{27}Mg$	-4.065	0.266396	4.1637	0.244635
$^{28}Mg$	-3.93233	0.256062	4.02441	0.234787
$^{29}Mg$	-3.89795	0.246598	3.98355	0.226164
$^{30}Mg$	-3.87287	0.237936	3.95204	0.218274
$^{31}Mg$	-3.41668	0.224842	3.52235	0.206223
$^{32}Mg$	-2.96194	0.211646	3.09244	0.194095
$^{33}Mg$	-2.96276	0.206741	3.09102	0.189597
$^{34}Mg$	-2.96402	0.202127	3.08998	0.185357
$^{35}Mg$	-2.96363	0.197607	3.08718	0.18121
$^{36}Mg$	-2.96752	0.193359	3.08865	0.177322
$^{37}Mg$	-2.96752	0.189208	3.08637	0.173515
$^{38}Mg$	-2.97189	0.185226	3.08797	0.169881
$^{39}Mg$	-2.97547	0.181501	3.08903	0.166466
$^{40}Mg$	-2.98107	0.17785	3.09205	0.163137

where  $f(r) = [1 + \exp(\frac{r-R}{a})]^{-1}$  and  $R = r_0 A^{(1/3)}$ . The first term of equation (21) contains the central potential, second term contains spin orbital part and the last term of the equation contains Coulomb part of potential.  $A$  be the mass number of nucleus. We fixed the value of  $r_0 = 1.2$  fm and diffuseness parameter "a" as 0.6 fm in our calculations.

Fig. 3 represents the values of  $\sigma_R$  for  $^{24-40}Mg+^{12}C$  reactions at  $E_{Proj}=240$  AMeV as a function of A of projectile nucleus. The calculated values of  $\sigma_R$  in the figure show a remarkable agreement with the experimental data except for the case of  $^{37}Mg$ , which support the success of RMF densities for the study of reaction dynamics. One may see some deviation particularly for higher Mg isotopes and  $^{37}Mg$  projectile. This difference in theoretical and experimental data for  $^{37}Mg$  nucleon is of further significance which seem to suggest that, it exhibits unusual structure

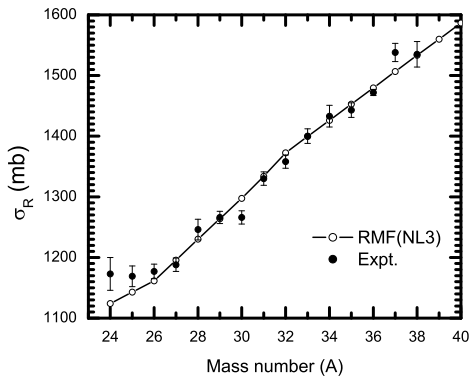


FIG. 3: Reaction cross section for  $^{24-40}\text{Mg}$  as projectile with  $^{12}\text{C}$  target nucleus at  $E_{proj} = 240$  A MeV. The experimental data are also given for comparison [10].

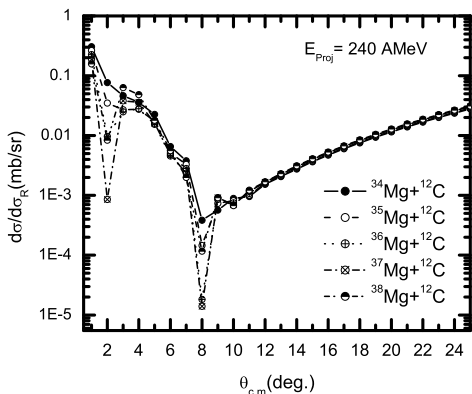


FIG. 4: The values of angular elastic differential cross section for  $^{34-38}\text{Mg} + ^{12}\text{C}$  reactions at  $E_{proj} = 240$  A MeV.

and hence needs further investigation. This point is explored in further discussion.

Fig. 4 shows the angular elastic differential cross sections of  $^{34-38}\text{Mg}$  projectiles on the carbon target at  $E_{proj} = 240$  A MeV. The inspection of the figure suggest that, two dip positions are observed at an angles  $\theta_{c.m.} = 2^\circ$  and  $8^\circ$ . One may also observe that the large dip appeared for  $^{37}\text{Mg}$  and  $^{38}\text{Mg}$  at these angles. Specifically speaking, the largest dip at  $^{37}\text{Mg}$  projectile may be associated with the loosely bound structure of this nucleus. The above observations give indication of halo behavior of  $^{37}\text{Mg}$ .

For further study of the case of  $^{37}\text{Mg}$  projectile, we have used Glauber formalism with two body (core+nucleon) system. Further details of the calculations can be seen in [25, 26]. Fig. 5 represents the calculated values of  $\sigma_R$  (in mb) and  $r_{rms}$  (in fm) for the  $^{37}\text{Mg}$  projectile. The upper panel of Fig. 5 presents the root mean square radius  $r_{rms}$  and lower panel represents  $\sigma_R$  for  $^{37}\text{Mg}$  as a projectile over the  $^{12}\text{C}$  target at energy 240 A MeV as a function of diffuseness parameter 'a' in fm. We have tried to fit the reaction cross section for  $^{37}\text{Mg}$  projectile at different values of diffuseness param-

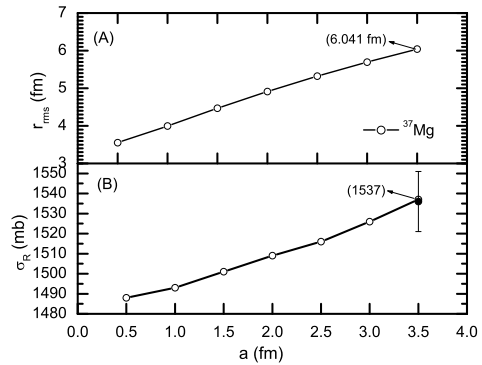


FIG. 5: (A) Upper panel of the figure show the rms radius ( $r_{rms}$ ) in fm and (B) lower panel show the values of reaction cross section  $\sigma_R$  in mb as a function diffuseness parameter 'a' in fm for  $^{37}\text{Mg}$ .

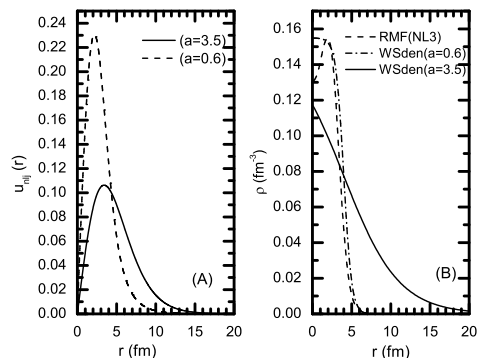


FIG. 6: (A) Comparison of single particle wave function for different values of diffuseness parameter 'a' and (B) Comparison of the Wood Saxon densities with different diffusion parameter and RMF(NL3) density of  $^{37}\text{Mg}$  as function of radial distance in fm.

eter. It is clear from the figure that the reaction cross section and diffuseness parameter are linearly dependant to each other. The value of  $\sigma_R$  obtained at diffuseness parameter = 3.5 fm is 1537 mb, which is well comparable to the experimental observation  $1536 \pm 15$  mb. Hence the lower panel of the figure shows that the value of reaction cross section fit with the experimental value at  $a = 3.5$  fm. The upper panel of the figure shows the rms radius values of core+nucleon system as a function of diffuseness parameter. We observed that the value of root mean square radius of projectile (core + nucleon) at  $a = 3.5$  fm is 6.041 fm. Thus the large value of reaction cross section has direct consequence to their large radius and halo nature of  $^{37}\text{Mg}$  isotopes.

Fig.6 represents the comparisons of wave function for different value of diffuseness parameters and RMF density for  $^{37}\text{Mg}$  with Wood-Saxon density having diffuseness parameter 0.6 fm and 3.5 fm. The left side of the figure show variation of single particle wave function with radial distance for different values of diffuseness parameter. This figure suggest that the wave function is more

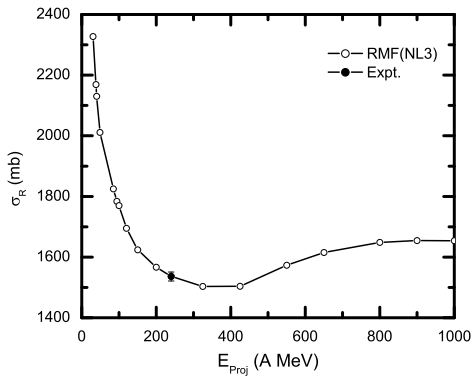


FIG. 7: Variation of Total reaction cross sections for  $^{37}\text{Mg}$  as function of  $E_{Proj}$ .

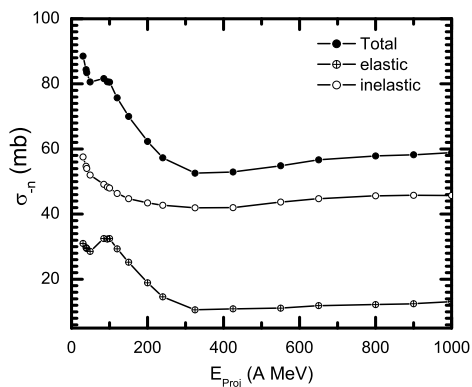


FIG. 8: One neutron removal cross section for the reaction  $^{37}\text{Mg}+^{12}\text{C}$  reaction including elastic and inelastic part as a function of  $E_{Proj}$  A MeV

steeper at diffuseness value of 0.6 fm where as more broader at 3.5 fm. The right side of this figure show that the behavior of Wood-Saxon density is similar to RMF at  $a=0.6$  fm. At the value of ' $a = 3.5$  fm', we get a long extension of density even beyond  $\sim 15$  fm, further suggesting the possibility of a halo structure of

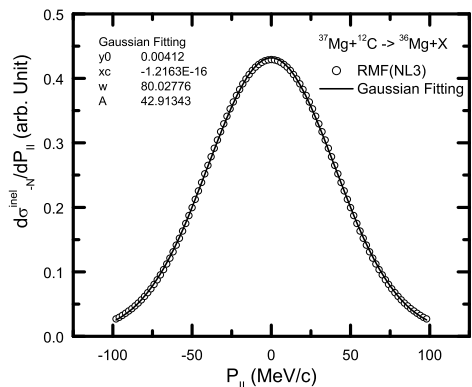


FIG. 9: Longitudinal momentum distribution of  $^{36}\text{Mg}$  from the  $^{37}\text{Mg}+^{12}\text{C}$  at projectile energy 240 A MeV.

$^{37}\text{Mg}$  nucleus. Although, this large value of  $a = 3.5$  fm looks unusual, but still be relevant for exotic nuclei exhibiting halo structure. For further significance of higher diffuseness parameter " $a$ ", one need to have extensive investigation by addressing reaction dynamics involving various halo nuclei. We have fitted density with a Wood-Saxon form taking variation in diffuseness parameter ' $a$ '. Then, we used these densities in the reaction calculation to evaluate the reaction cross-section  $\sigma_R$ . We find that the fitted density reproduce the experimental data for  $^{37}\text{Mg}$  at  $a = 3.5$  fm.

Fig. 7 represents the variation of reaction cross section as a function of projectile energy for 30-1000 A MeV using wave function with  $a=3.5$ . The experimental values are also given for comparison. Fig. 8 shows the one neutron removal cross section for  $^{37}\text{Mg}+^{12}\text{C}$  reaction as a function of  $E_{Proj}$ . One neutron removal cross section consists of both elastic and inelastic component. It is clear from the figure that the inelastic component in neutron removal cross section dominate over their elastic component at  $E_{Proj}=240$  A MeV. The trend of reaction cross section in figure 7 and one neutron removal cross section in figure 8 are similar, but small hike is appeared in one neutron removal cross section at  $E_{Proj}=100$  A MeV, because of its elastic component.

Fig. 9 show the calculated longitudinal momentum distribution of  $^{36}\text{Mg}$  core for the reaction  $^{37}\text{Mg}+^{12}\text{C}$  at  $E_{Proj}=240$  A MeV. The trend of distribution exhibits the Gaussian pattern. So we compare our calculated values of longitudinal momentum distribution using RMF densities with in Gaussian function. The circle points show the calculated values of momentum distribution of one nucleon from the  $^{37}\text{Mg}$  projectile and solid line is the fitted gaussian curve. By fitting curve the observed value of FWHM comes out to be 80.02 MeV/c.

#### IV. SUMMARY

In summary, we have calculated the ground state properties of Mg isotopes and also studied the reaction cross sections of these isotopes taken as projectile from the valley of stability to drip line region with stable  $^{12}\text{C}$  target at  $E_{proj}$  240 A MeV. We found remarkable agreement of ground state properties of Mg-isotopes with available data. The estimated values of reaction cross section using densities from RMF formalism are nicely compered with the experimental data. The excellent agreement of estimated reaction cross section values except for  $^{37}\text{Mg}$  isotope is an evidence of predictive power of RMF. The skin effect variation with mass number is studied in context of density profile. The study of angular elastic differential cross section for  $^{34-38}\text{Mg}$  and further investigation with Glauber two body calculation also support the halo status of  $^{37}\text{Mg}$ . Subsequently we examined the halo status of  $^{37}\text{Mg}$  and it seems justified from its higher magnitude of rms radius  $\sim 6.041$  fm and small value of FWHM (80.02 MeV/c) of longitudinal momentum distribution.

- 
- [1] I. Tanihata et al., *Phys. Lett. B* **287** (1992) 307.
- [2] B. Paes, J. Lubian, P. R. S. Gomes and V. Guimaraes, *Nucl. Phys. A* **890-891** (2012) 1-10.
- [3] D. Bazin, B. A. Brown et al., *Phys. Rev. Lett.* **74** (1995) 18.
- [4] K. Tanaka et al., *Phys. Rev. Lett.* **104** (2010) 062701.
- [5] N. Kobayshi et al., arXiv: 1111.7196 v1 [Nucl. ex] (2011).
- [6] A. Ozawa et al., *Phys. Rev. Lett.* **84** (2000) 24.
- [7] I. Tanihata et al., *Nucl. Phys. A* **682** (2001) 114c.
- [8] I. Hamamoto, *Phys. Rev. C* **81** (2010) 021304(R); Y. Urata, K. Hagino and H. Sagawa, *Phys. Rev. C* **83**(2011) 04130; K. Minomo, T. Sumi, M. Kimura, K. Ogata, Y. R. Shimizu and M. Yahiro, *Phys. Rev. C* **84** (2011) 034602.
- [9] M. Takechi et al., *Phys. Lett. B* **707** (2012) 357-361.
- [10] M. Takechi, S. Suzuki et al., *EPJ Web of conference* **66** (2014) 02101. M. Takechi et al., *Phys. Rev. C* **90**, (2014) 061305.
- [11] S. Watanabe, K. Minomo et al., *EPJ Web of conference* **66** (2014) 03095.
- [12] R. N. Panda, Mahesh K. Sharma and S. K. patra, *Mod. Phys. Latt. A* **29** (2014) 1450013.
- [13] R. J. Glauber, *Phys. Rev.* **100** (1955) 242, *ibid*, Lectures on theoretical physics, edited by W. E. Brittin and L. C. Dunham (Int. Sc., New York) **1** (1959) 315.
- [14] P. J. Karol, *Phys. Rev. C* **11** (1975) 1203.
- [15] J. Chauvin et. al, *Phys. Rev. C* **28** (1983) 1970.
- [16] G.A. Lalazissis, J. König, and P. Ring, *Phys. Rev. C* **55** (1997) 540.
- [17] M. Buenerd et. al, *Nucl. Phys. A* **424** (1984) 313.
- [18] W. Pannert, P. Ring and J. Baguta, *Phys. Rev. Lett.* **59**, (1987) 2420.
- [19] J. Baguta and A. R. Bodmer, *Nucl. Phys. A* **292**, (1977) 413.
- [20] S. K. Patra and C. R. Praharaaj, *Phys. Rev. C* **44**, (1991) 2552.
- [21] M. Del Estal, M. Centelles, X. Vinas and S. K. Patra, *Phys. Rev. C* **63**, (2001) 024314.
- [22] P. Ring, *Prog. Part. Nucl. Phys.* **37**, (1996) 193.
- [23] W. Horiuchi, Y. Suzuki, B. Abu Ibrahim and A. Kohama, *Phys. Rev. C*, **75** (2007) 044607.
- [24] A. Shukla, B. K. Sharma, R. Chandra, P. Arumugam and S. K. Patra, *Phys. Rev. C* **76** (2007) 034601.
- [25] B. Abu-ibrahim, Y. Ogawa, Y. Suzuki and I. Tanihata *Comut. Phys. Commun.* **151** (2003) 369.
- [26] Mahesh K. Sharma and S. K. Patra, *Phys. Rev. C* **87** (2013) 044606, and references there in.